Korean J. Chem. Eng., 40(11), 2751-2758 (2023)
DOI: 10.1007/s11814-023-1483-2

pISSN: 0256-1115
eISSN: 1975-7220

The importance of deprotonation of copper oxyhydroxide on its activity towards water oxidation reactions

Jia Guo[*,], Naeem Akram[*,***], Liugen Zhang[*], Xianglei Cao[*], Guangyao Wang[*], Ali Ahmad[***], Junmin Niu[**], Muhammad Saad Mansha[***], Yi Zhang[****], and Jide Wang[*,†]**

*Key Laboratory of Oil and Gas Fine Chemicals, Ministry of Education & Xinjiang Uygur Autonomous Region, College of Chemical Engineering and Technology, Xinjiang University, Urumqi, 830046, China
**Xinjiang Energy Co., LTD
***School of Chemical Engineering, Minhaj University Lahore, Lahore 54000, Punjab, Pakistan
****Hunan Provincial Key Laboratory of Efficient and Clean Utilization of Manganese Resources, College of Chemistry and Chemical Engineering, Central South University, Changsha 410083, Hunan, China
(*Received 12 January 2023 • Revised 4 April 2023 • Accepted 1 May 2023*)

Abstract−This work reveals a schematic strategy to massively fabricate a series of OH-riched copper oxides (CuO-OH), which could be used as highly efficient chemo catalysts for water oxidation reaction (WOR). The results indicate that the as-prepared CuO-OH exhibited excellent catalytic activity (2,900 $\mu mol \cdot h^{-1} \cdot g^{-1}$) toward water oxidation, far higher than the pure CuO formed through calcination. According to the radical capture results and the DRIFTS, XRD, and Raman spectra data, sulfate radicals were the main active species. Subsequent data of BET, HR-TEM, and FT-IR spectra reveal that the CuO-OH could activate persulfate ions in the dark to produce sulfate radicals efficiently at room temperature and promote the sulfate radicals to carry out immediately to hydroxide-mediated deprotonation steps in WOR. Based on the results above, a mechanism is proposed.

Keywords: CuO-OH, Water Oxidation Reactions (WOR), Chemocatalytic, Deprotonation

INTRODUCTION

The energy crisis and environmental degradation have been major issues for the last few decades; thereby, cheaper, sustainable, clean energy sources are urgently demanded [1-3]. Hydrogen (H_2), characterized as pollution-free, high enthalpy heat, and high energy output efficiency, has attracted widespread interest for years [3,4]. Water splitting ($2H_2O \rightarrow 2H_2+O_2$) reaction is regarded as the most effective way to obtain H_2 [5-8]. The half-reaction (water oxidation reaction (WOR)) involves a four-electron transfer process, leading to the main thermodynamics and kinetics (1.23 V vs. NHE) restricts toward water splitting. Numerous efforts have been attempted to lower the potential barrier of the WOR by seeking effective catalysts to accelerate the reaction, including electrochemical-catalytic, photocatalytic, and chemical methods [5,8,9]. Among them, chemocatalytic WOR is not complicated since it has a relatively simple process design and fewer requirements for catalysts [10-12].

The earliest research work on chemo catalytic WORs was reported in 1968 when Glikman et al. discovered that Mn oxides could oxidize the water in the presence of cerium(IV) ammonium nitrate (CAN) [12]. Subsequently, the catalytic properties of some precious metals, such as Ru and Ir, have been verified. In 2005, Zong and Thummel first reported that mononuclear Ru-based complexes served as excellent water oxidation catalysts in Ce (IV)-CF_3SO_3H solution (pH=1.0) [10]. In 2008, Bernhard and his group first reported a series of cyclometalated iridium (III) aqua complexes that exhibited excellent catalytic properties in WOR when using Ce(IV) as the oxidant [13]. Given commercial profit and industrial availability, numerous efforts have been made to replace precious metals with earth-abundant elements. Co [14] and Fe [11] based compounds were commendable water oxidation catalysts (WOC). It is necessary to point out that CAN is the most often used oxidant in the reactions mentioned above [10,12,13], and it is only stable at low pH solutions. Hence, another oxidant is required, whose oxidation capacity should not be significantly affected by acidity and alkalinity of a solution. Sodium persulfate is a powerful intrinsic oxidant, with a reduction potential of 2.0 V vs. NHE, approximately. Moreover, its kinetic stability is quite satisfactory. Apart from that, sulfate radicals can also be produced using persulfate under the action of a catalyst, which has a higher potential, i.e., ~2.4 V vs. NHE, to oxidize water and produce a relatively benign sulfate [15-17]. Owing to such properties of persulfate, mesoporous $Au/BiFeO_3$ combined with persulfate as an oxidant was used to drive water oxidation with a high oxygen rate (586 $\mu mol \cdot h^{-1} \cdot g^{-1}$) [6].

Persulfate is stable in water solution, and there needs a catalyst to activate it, for instance, converting it to sulfate radicals to oxidize the reactants. There are two proposed mechanisms for converting persulfate to sulfate radicals. One is that the persulfate ions are directly activated by heat or UV-visible light, and the other is that the transition metals provide the electrons to persulfate ions resulting in the generation of sulfate ions and sulfate radicals [17-22].

†To whom correspondence should be addressed.
E-mail: awangjd@sina.cn

Recently, metal oxyhydroxides have attracted special attention in WOR owing to their exceptional physical and chemical properties [23-26]. Koper et al. presented an in situ surface enhanced Raman spectroscopy study (SERS) of the pH-dependent interfacial changes of the NiOOH catalyst under the working conditions, pointing out that the deprotonation of NiOOH produced negatively charged (or proton-deficient) surface species, which were responsible for the enhanced electrochemical WOR activity of NiOOH in highly alkaline pH [25]. Boettcher and co-workers proposed a mechanism that Fe had been predicted to increase the catalytic activity of $Ni(OH)_2$/NiOOH for the electrochemical WOR [24]. In addition, Vela et al. reported that cobalt oxyhydroxide nanocrystals could be facilely gained via photochemical and thermal synthesis, but they reported no related mechanism study [26]. Despite these proposed mechanisms that may reasonably explain the excellent oxygen evolution of metal oxyhydroxide, insights into the catalytic pathway and experimental evidence of the proposed mechanism are still needed.

This paper uses a simple and comparative strategy to evaluate the deprotonation mechanism of OH - riched copper oxides (CuO-OH) and pure CuO in persulfate/ sodium hydroxide solution for chemocatalytic WOR, respectively. It was excitingly found that the as-prepared CuO-OH exhibited excellent catalytic performance, and the oxygen-generating rate was as high as 2,900 $\mu mol \cdot h^{-1} \cdot g^{-1}$, while the pure CuO without hydroxy displayed much poorer activity in WOR. Subsequently, we noticed that the CuO-OH could activate persulfate in the dark and at room temperature to produce sulfate radicals. The synergistic effect makes the sulfate radicals the dominant oxidant in WOR. Based on the Raman spectra measurement, XRD FT-IR results, and the previous deprotonation mechanism of metal oxyhydroxides by SERS [25], a new mechanism was proposed in which CuO-OH can serve as an activator for persulfate in WOR. We expect that this contribution will provide a pathway for designing and developing new chemocatalytic water oxidation catalysts.

EXPERIMENTAL DETAILS

1. Materials

All the chemicals used in this work were of analytical grade and used without further purification. $Na_2S_2O_8$ was purchased from ACROS (Fisher Scientific Worldwide Co., Ltd, Shanghai). Sodium citrate dehydrate ($C_6H_5Na_3O_7 \cdot 2H_2O$), NaOH, $CuSO_4 \cdot 5H_2O$, $Cu(CH_3COO)_2 \cdot H_2O$, $Cu(NO_3)_2 \cdot 3H_2O$ methanol (MA) and *test*-butyl alcohol (TBA), ethylene glycol (EG), glacial acetic acid were supplied by Adamas (Titan Scientific Co. Ltd, Shanghai) and Sigma (Sigma-Aldrich Co.).

2. Preparation of CuO Nanostructures

2-1. Synthesis of CuO via Chemical Precipitation Method

The preparation was according to the reported literature [27]. 1.20 g of $Cu(CH_3COO)_2 \cdot H_2O$ was dissolved in 300 mL of distilled water in a round-bottomed flask equipped with a refluxing device. 1.00 mL glacial acetic acid was added by providing continuous magnetic stirring; a blue solution appeared. This blue solution was then heated to 40 °C, 0.80 g of NaOH (s) was quickly added into the solution, and then again heated to 100 °C for 30 min, where a large amount of brownish-black precipitate was produced. After cooling to room temperature, the precipitate was centrifuged, washed once with distilled water, and dried at 80 °C in a vacuum oven for the whole night. This sample is labeled as catalyst 1.

2-2. Synthesis of CuO via a Microwave-assisted Method

The preparation was according to the reported literature [28]. Typically, 2.50 g of $CuSO_4 \cdot 5H_2O$ and 8.823 g of $C_6H_5Na_3O_7 \cdot 2H_2O$ were dissolved in 98 mL of distilled water, followed by the addition of 2 mL of EG, along with magnetic stirring for 30 min. Then 60 mL of NaOH (10.00 g, about 35 s) solution was added to form a clarified dark-blue solution. After stirring for 60 min, the solution was transferred to a Teflon autoclave. The vessel was sealed and placed in the programmable microwave system equipped with a magnetic stirrer. The oven was heated to 120 °C for 5 min by microwave irradiation and maintained there for another 15 min. After cooling to room temperature, the precipitate was collected by vacuum filtration, washed with water and ethanol, and dried at 80 °C in a vacuum oven for the whole night. This sample is labeled as catalyst 2.

Catalyst 3 was also synthesized the same way as catalyst 2; however, the only difference in the synthesis method was that it was synthesized without the addition of $C_6H_5Na_3O_7 \cdot 2H_2O$.

2-3. Synthesis of CuO via Calcination Method

The preparation was according to the literature with a little modification [29]. Catalyst 4 was obtained via calcination of $Cu(NO_3)_2 \cdot 3H_2O$ in the muffle furnace with temperature programming. Typically, 1.0 g $Cu(NO_3)_2 \cdot 3H_2O$ was first heated to 150 °C and maintained at this temperature for 120 min. Then the temperature was raised to 400 °C for another 240 min. The heating rate was 10 °C·min^{-1} during the whole process.

3. Characterization

BET surface areas were measured with Brunauer-Emmett-Teller (BET) equipment provided by JW-BK, China. Characterization powder X-ray diffraction (PXRD) data were acquired using a Rigaku D/max-ga X-ray diffractometer, Japan, at a scan rate of 6° per minute in 2 ranging from 5 degrees to 80 degrees with Cu K radiation (=1.54178 Å). Hitachi SU8010 microscope, Japan, was used and operated at 5 kV to obtain images of field emission scanning electron microscopy (FESEM). The concentration of copper ion was measured by atomic absorption spectrometry (AAS) (Agilent 240 FS AA, USA). In situ DRIFTS measurements were conducted using a Tensor II FT-IR spectrometer EQUINOX-55 (Bruker, Germany) equipped with an in situ diffuse reflectance cell (Harrick). The Raman-scattering (LabRAM HR Evol, HORIBA) measurements were carried out at room temperature with the He/Ne laser (532 nm) at 2 cm^{-1} in the range between 40 and 1,000 cm^{-1}. Transmission electron microscopy (TEM) was carried out by using JEM-2010F (Eurofins Nanolab Technologies, USA) coupled with a digital charge device. The electron spin resonance (ESR) measurements were used in a JES FA300 (Jeol, Japan) Spectrometer, using 5, 5-Dimethyl-1-Pyrroline-N-Oxide (DMPO) as the radical capture agent.

4. Water Oxidation Reaction

The chemocatalytic WOR was studied as follows. The reaction vessel (20 mL) contained 10 mL of a certain concentration of NaOH solution and a certain concentration of $Na_2S_2O_8$ at room temperature, then proceeded with the addition of a specific amount of as-

prepared catalyst in the solution under agitation. The rubber septum was used to seal the reaction vessel and purged with Ar gas for 3 min to remove the air present in the headspace of the vessel. To avoid the effect of light, the vessel was covered with tin foil paper. The evolved oxygen was detected and analyzed using gas chromatography with a thermal conductivity detector (Shimadzu GC-14B) and a 5 Å molecular sieve column (2 m×4 mm) having Ar as a carrier gas.

RESULTS AND DISCUSSION

1. Characterization of CuO Nanoparticles

The crystal phases of four individual morphologies of CuO were investigated by XRD analysis (Fig. 1(a), (c), (e), and (g)). The diffraction data followed JCPDS cards of CuO (catalyst 1: JCPDS 48-1548; catalyst 2: JCPDS 80-1916; catalyst 3: JCPDS 72-0629; catalyst 4: JCPDS 80-0076). All the pointed peaks indicated that CuO was well-crystallized, and no impurity peak could be observed in the XRD pattern.

FESEM was used to analyze the morphologies of CuO obtained via different synthetic methods. The FESEM images revealed that their morphologies were quite different (Fig. 1(b), (d), (f), (h)) due to their diverse synthetic methods.

Catalyst 1 presents a shuttle-like shape with a smaller size ranging from 200-450 nm, and its surface is rough due to numerous small raised bumps (Fig. 1(b)). The CuO product prepared by the microwave method shows a much larger size than the former one, which reaches the micron scale.

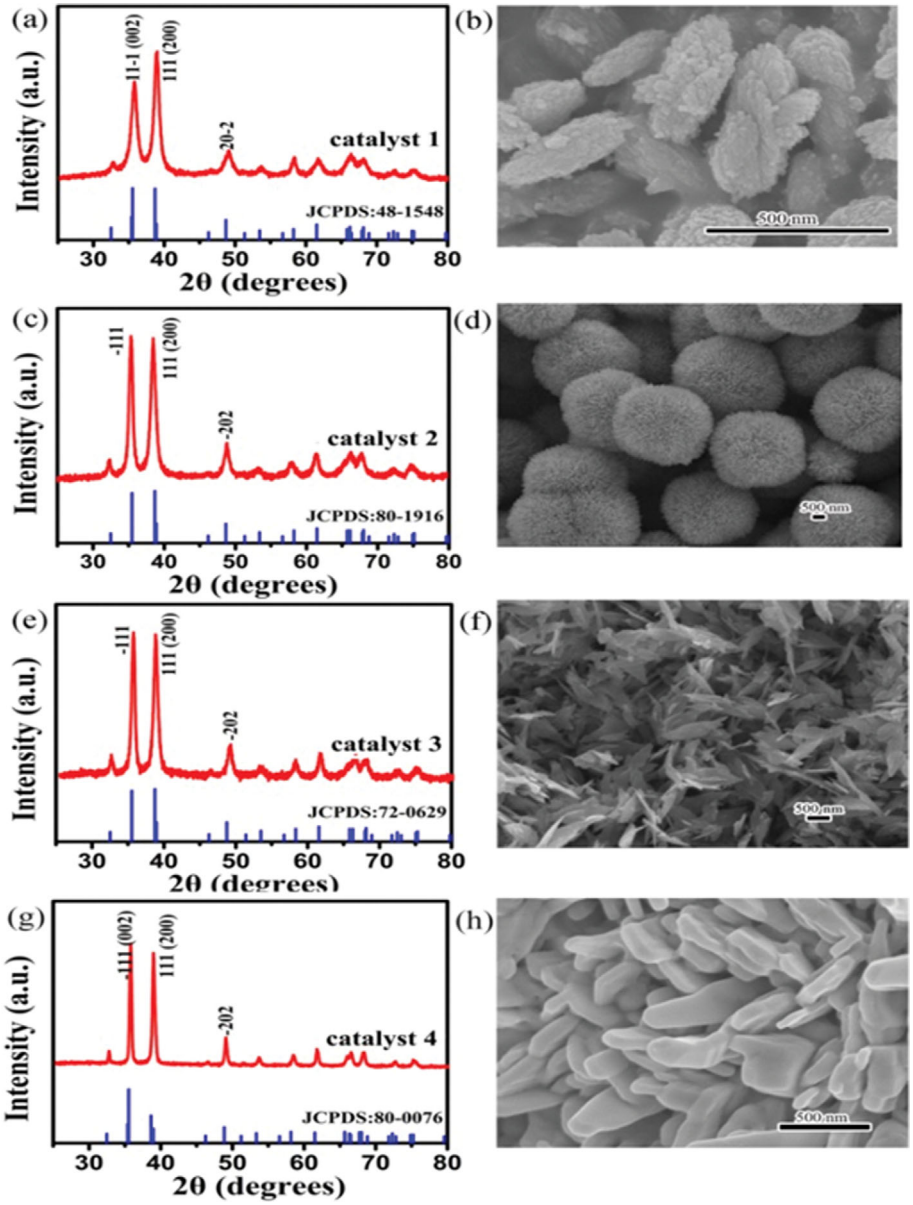

Fig. 1. XRD patterns and FESEM images of various morphologies of CuO (Catalyst 1: (a) and (b); catalyst 2: (c) and (d); catalyst 3: (e) and (f); catalyst 4: (g) and (h)).

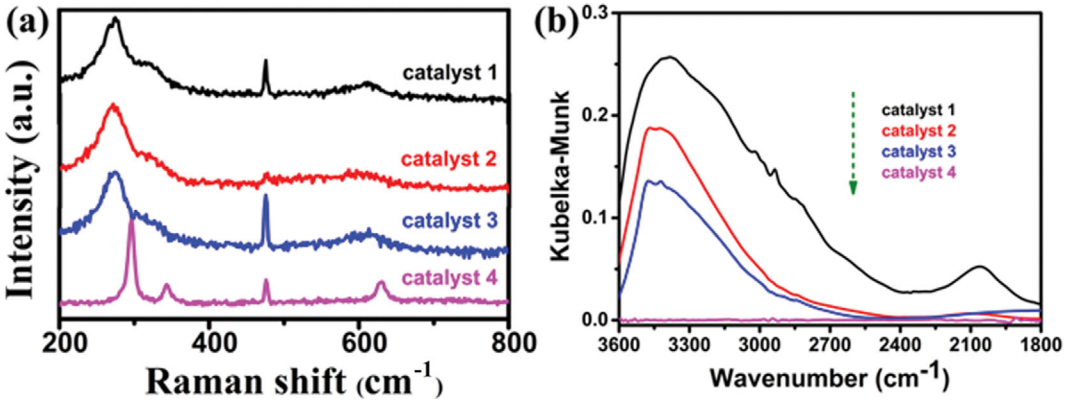

Fig. 2. (a) Raman spectrum of different catalysts of CuO; (b) In-situ FT-IR spectra of different morphologies of CuO.

In the presence of $C_6H_5Na_3O_7{\cdot}2H_2O$, the shape of CuO is like a sea urchin (catalyst 2) with a fairly uniform size of 3 mm (Fig. 1(d)). Without $C_6H_5Na_3O_7{\cdot}2H_2O$, catalyst 3 appears as long striped, like a thin leaf (Fig. 1(f)). The morphology of catalyst 4 presents an irregular block-like with a smooth surface (Fig. 1(h)).

Raman and DRIFTS measurements were carried out to certify whether there were any functional groups on the surface of CuO. Fig. 2(a) was the Raman spectra of four products. CuO has two molecules per primitive cell and C_6^{2h} space group symmetry. The equation associated with a primitive cell's lattice vibrations is as follows:

$$\Gamma_{RA}=4A_u+5B_u+A_g+2B_g \quad (1)$$

Group theory predicts 12 vibration modes, three of which are active Raman modes (A_g+2B_g), and the others are infrared and acoustic modes ($3A_u+2B_u$) and (A_u+2B_u).

The Raman spectra show the A_g active mode of CuO nanoparticles at the strongest peak, i.e., 274 cm^{-1}, where A_g mode corresponds to phase rotations and stretching vibrations and the observed pattern well matches the previously reported literature [30]. The characteristic peak of catalyst 4 moves to a high wave number (296 cm^{-1}), which may be related to its different surface state.

The DRIFTS measurements were conducted (Fig. 2(b)). The broad peak between 3,510 and 3,200 cm^{-1} is due to surface OH singly coordinated to CuO. From the results, it can be concluded that CuO-OH has been expediently synthesized [31]. However, pure CuO can be obtained by the calcination method in a muffle furnace. In this work, three different morphologies of CuO-OH and pure CuO were successfully synthesized.

2. Catalytic Performance in WOR

The O_2 contents in the headspace of the bottle were analyzed by GC. As the results are shown in Fig. 3, four catalysts display different performances since different amounts of O_2 evolution were observed. The maximum oxygen rate of catalyst 1 can reach as high as 1,833 $\mu mol{\cdot}h^{-1}{\cdot}g^{-1}$ (Fig. 3) and 2,900 $\mu mol{\cdot}h^{-1}{\cdot}g^{-1}$ (ESI Fig. S2). Catalyst 2 and catalyst 3 also display good catalytic activities. However, catalyst 4 exhibits poor catalytic activity in WOR. The results are consistent with those shown in Fig. 2(b), indicating that the hydroxyl group on the surface of copper oxide plays a crucial role in the catalytic reaction. There was no O_2 evolution when only $Na_2S_2O_8$ or any catalyst was used.

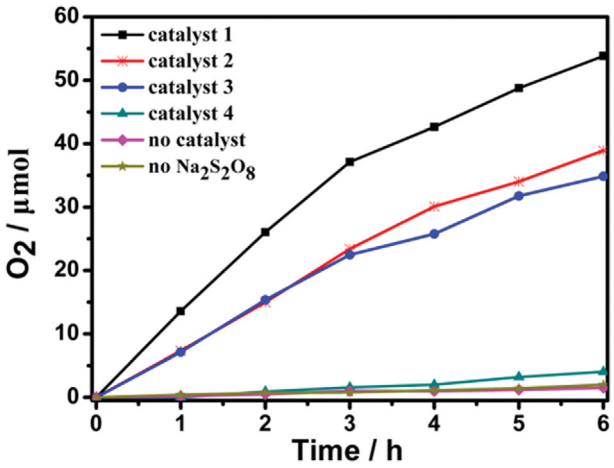

Fig. 3. Time courses of O_2 evolution in NaOH solution (0.10 M, 10 mL) containing $Na_2S_2O_8$ (20 mM) and catalyst (5 mg) at room temperature.

As shown in Fig. 3, the catalytic property shown by catalyst 1 was the best of the four, so several control experiments were performed. NaOH plays an important role, and its role was deduced in the following mechanism discussion.

After comparing the effects of various NaOH concentrations (0.01-1.00 M), 0.10 M NaOH was selected as the optimal one (ESI Fig. S1). Then, the optimal $Na_2S_2O_8$ concentrations and most suitable catalyst dosage were 60 mM and 10 mg, respectively (Fig. S2-S3). Finally, the stability of catalyst 1 was evaluated, and even after the fifth run, it still exhibited excellent catalytic activity (ESI Fig. S4-S6). The leached-out experiment was carried out. The results of AAS indicated that a minimal amount of Cu^{2+} (only 0.10%) exuded from catalyst 1. Then the supernatant was removed and another 20 mM $Na_2S_2O_8$ was added, and after reacting for 6 h, only trace amounts of O_2 could be detected. The results demonstrated that the real catalyst was CuO rather than Cu^{2+}.

3. Catalytic Performance

3-1. Factors Affecting the Catalytic Activity

The four catalysts with different morphologies exhibit distin-

Table 1. BET surface areas of different morphologies of catalysts

Sample	BET surface area ($m^2 \cdot g^{-1}$)
Catalyst 1	50.7
Catalyst 2	10.9
Catalyst 3	18.3
Catalyst 4	27.8

guishing catalytic properties, especially catalyst 4. Several characterizations were carried out to reveal the main factor affecting the catalytic performance.

The data of BET surface areas are listed in Table 1. The results show that catalyst 1 occupied the largest surface areas, attributed to the small size and the small particles on the rough surface. Catalyst 4 had the second-largest surface area, but its catalytic performance was the worst. The results indicate that BET surface area was not the main factor that affected the catalytic performance.

Then from the HR-TEM images, the distance of lattice fringes was measured. Fig. 4(a) is the image of catalyst 1 with the lattice spaces of 0.23 nm, which was matched well with the (1 1 1) plane. The lattice spaces of 0.27 nm correspond to the (1 1 0) facet of catalyst 2 (Fig. 4(b)). Catalyst 3 (Fig. 4(c)) presents a (–1 1 1) plane for the lattice spaces of 0.25 nm. The lattice spaces of catalyst 4 (Fig. 4(d)) was 0.23 nm, which is consistent with the (1 1 1) facet. The results of HR-TEM suggest that the catalytic activity of different morphology of catalysts has no direct relationship with the crystal lattice plane.

Comparative experiments were further done. Catalyst 1 was calcified under the same reaction condition as catalyst 4.

Fig. 5(a) and (b) present the FESEM images of catalyst 1 before and after calcification, respectively. The surface after calcification became much smoother, with a smaller surface area (24.0 $m^2 \cdot g^{-1}$), and the catalytic activity was much poorer than that before calcification (Fig. 5(c)). Fig. 5(d) shows the FT-IR spectra of catalyst 1 before and after calcification. The very broad peak between 3,510 cm^{-1} and 3,200 cm^{-1} disappeared after calcification due to the surface OH coordinated to CuO. These results may conclude that the surface OH of the CuO was the critical factor that determined the catalytic performance. This conclusion can be further confirmed in Fig. 2(b), Fig. 3, and Table 1. Fig. 2(b) shows that the broad peak that appeared between 3,510 cm^{-1} and 3,200 cm^{-1} of catalyst 2 was more substantial than catalyst 3, which means the catalytic property of catalyst 2 was better than the catalyst 3 (Fig. 3), although the former had a larger BET surface area (Table 1).

3-2. Reaction Mechanism

To study which kind of radicals were generated in WOR, electron spin resonance (ESR) was performed by using 5,5-Dimethyl-1-Pyrroline-N-Oxide (DMPO) as the radical capture agent. Results of Fig. 6(a) depicting the presence of $SO_4^{\bullet-}$ and $HO^{\bullet}$ radicals and the rate of generation of these radicals firmly increased over time. These results evidently explain the key role of these radicals generated during the reaction, for O_2 evolution.

Ordinarily, persulfate ions in the presence of ultraviolet (UV) light, heat, and some metal catalysts can oxidize reductants by producing sulfate and hydroxyl radicals. Therefore, there are two types of active species (sulfate and hydroxyl radicals) in the WOR [32]. To investigate the main active species in WOR, two different radical capture reagents were used. Tert-butyl alcohol (TBA) and methanol (MA) were selected as the probe reagents for radicals in this study because they are stable in alkaline solutions. MA can combine hydroxyl and sulfate radicals, as it contains α-hydrogen, while TBA without α-hydrogen only immediately reacts with hydroxyl radicals [33].

In the beginning, to verify if the persulfate could be active in the alcohol to evolve the oxygen, the reaction conditions for the experi-

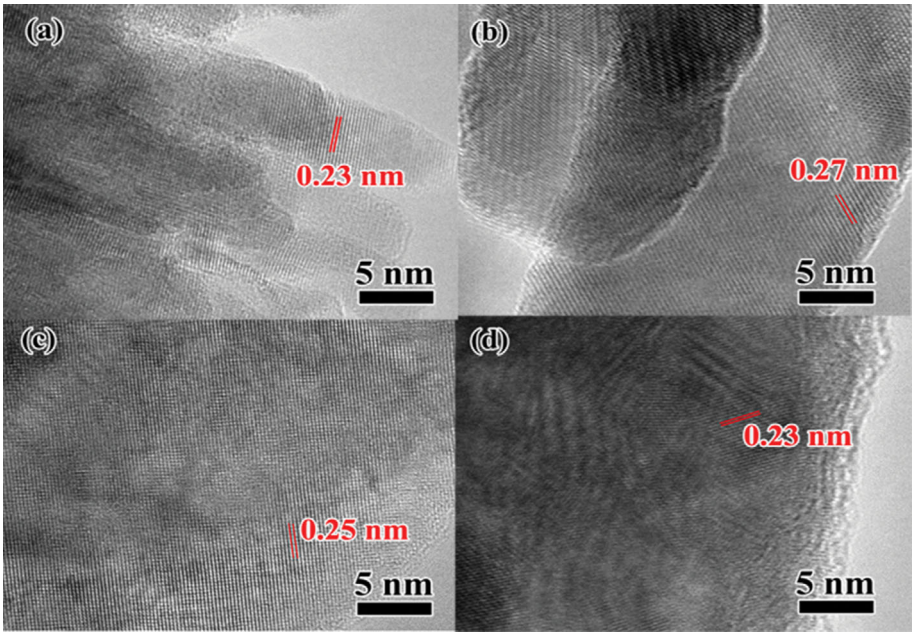

Fig. 4. High-resolution TEM images of different morphology of catalysts ((a) catalyst 1; (b) catalyst 2; (c) catalyst 3; (d) catalyst 4).

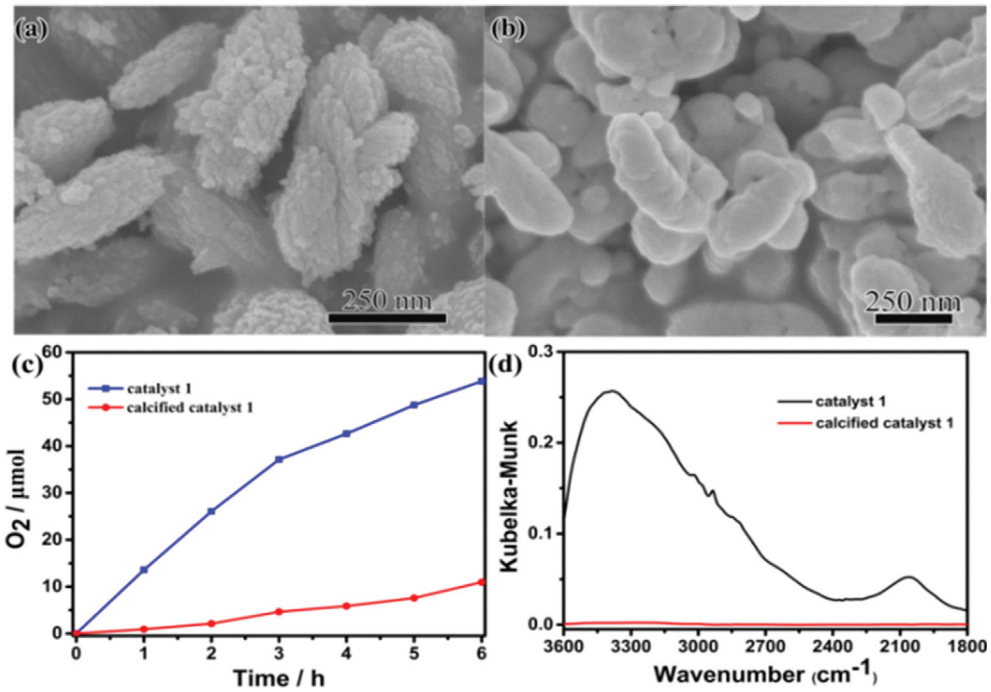

Fig. 5. (a) FESEM image of catalyst 1. (b) FESEM image of catalyst 1 after calcification. (c) Time courses of O_2 evolution in NaOH solution (0.10 M, 10 mL) containing $Na_2S_2O_8$ (20 mM) and catalyst (5 mg) at room temperature. (d) In situ FT-IR spectra of catalyst 1 before and after calcification.

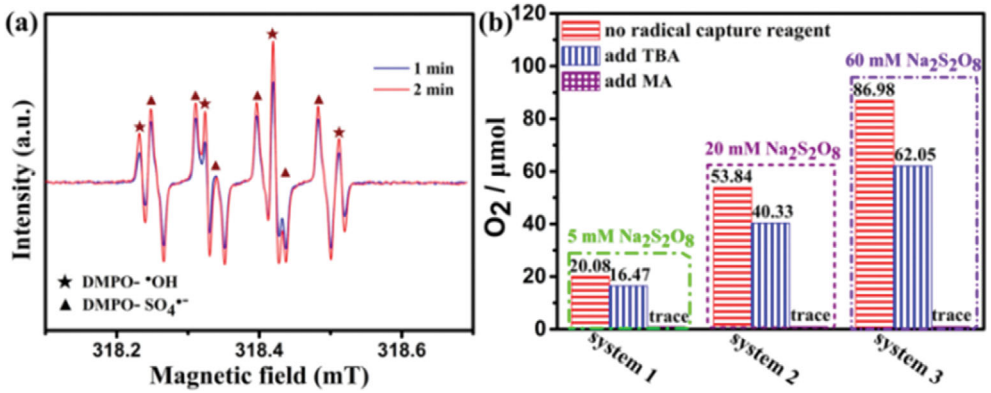

Fig. 6. (a) ESR spectra of DMPO trapped radical adducts. (b) Oxygen evolution is catalyzed by the catalyst and with radical capture reagents (Reaction condition: NaOH solution: 0.10 M, 10 mL; catalyst: 5 mg; vigorous stirring at RT; The concentration of MA and TBA were ten times the equivalent of $Na_2S_2O_8$).

ment were kept the same except that MA or TBA replaced the NaOH solution, and there was no oxygen evolved. Based on this result, we believe that MA and TBA would capture the radicals in WOR rather than be oxidized by persulfate to produce oxygen.

The amounts of O_2 generated after 6 h with radical capture reagents in different reaction systems are shown in Fig. 6(b). Reaction systems 1, 2, and 3 with varying concentrations of $Na_2S_2O_8$ (5, 20, and 60 mM) were studied to investigate the radical mechanism.

Take reaction system 1, for example. When there were no radical capture reagents in the reaction, the amount of O_2 evolved was 20.08 μmol after 6 hours. While adding TBA, O_2 was decreased to 16.47 μmol, and the yield of O_2 was kept at 83.0% compared to the former. This result was connected with the deficiency of hydroxyl radicals. In the presence of MA, only a trace amount of O_2 evolved in the reaction system.

Reaction systems 2 and 3 had similar results as that 1. The amounts of O_2 were 53.84 μmol and 86.98 μmol, respectively, when radical capture reagents were not used. In the presence of TBA, the amounts of O_2 were decreased to 40.33 μmol and 62.05 μmol, respectively, which kept 74.9% and 71.4% of O_2 evolved in reaction systems 2 and 3. Only a minute quantity of oxygen production was detected when MA was employed. These results indicated that when CuO-OH was used as a catalyst in WOR, the sulfate radicals produced were mainly used to evolve O_2 without transforming to $HO^{\bullet}$ radicals.

From these results, it could be concluded that the CuO-OH

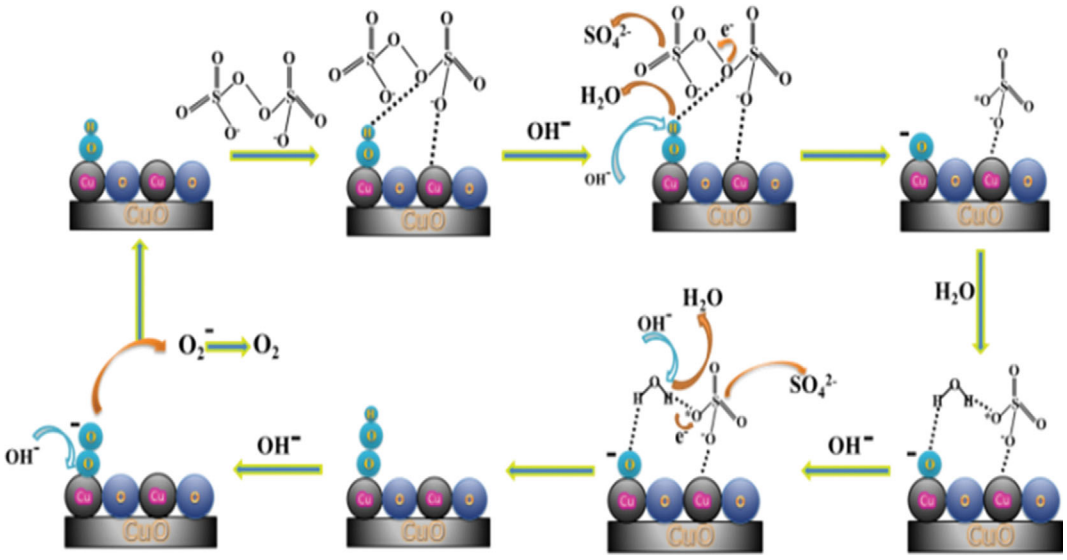

Fig. 7. Catalytic mechanism of CuO-OH in the water oxidation reaction.

could activate persulfate ions in the dark to produce sulfate radicals efficiently at room temperature. It promoted the sulfate radicals to immediately carry out the hydroxide-mediated deprotonation steps in WOR as the primary oxidant without evolving into hydroxyl radicals.

Based on the obtained results and proposed deprotonation mechanism by SERS [25], a mechanism of CuO-OH for activating persulfate in WOR could be proposed in Fig. 7. In the beginning, the persulfate interacted with the Cu and OH on the surface of CuO-OH, which activated persulfate ions to generate sulfate ions and sulfate radicals. Then a molecular H_2O participated in forming an aqua-complex. The nucleophilic attack of hydroxide allowed the sulfate radical on the surface of CuO-OH to accept an electron from H_2O to generate another sulfate and produce CuOOH on the catalyst's surface. The CuOOH could further form $CuOO^-$ and a hydroxide. The deprotonated negatively charged O_2^- present on the surface would evolve O_2 [25].

Based on this mechanism, it could be better understood that the primary oxidant in the WOR is the sulfate radicals rather than hydroxyl radicals, since the sulfate radicals produced were directly used to evolve oxygen instead of transforming to hydroxyl radicals. The catalyst showed its optimal catalytic performance in 0.1 M NaOH since the deprotonation of hydroxide promoted the WOR; however, when the concentration of NaOH is higher, this would produce excess CuO-OH and less Cu vacancy on the catalyst surface, which would be no good for connecting and activating persulfate. On the other hand, a strong alkalic solution would accelerate the corrosion of the catalyst.

CONCLUSIONS

Metal hydroxide and oxide are well-known as promising catalysts for water oxidation reactions (WOR), but their catalytic pathways are still under discussion. This paper proposes a simple and facile strategy to synthesize CuO-OH and pure CuO. The catalytic properties of as-prepared CuO-OH and pure CuO were examined in WOR, and the results revealed that CuO-OH exhibited excellent activity, while pure CuO showed much worse. BET and HR-TEM results disclosed that the surface area and the lattice plane were not the main factors that affected the catalytic performance. By comparing the catalytic performance of catalyst 1 before and after calcification, we discovered that the hydroxyl group on the catalyst's surface plays a crucial role in WOR. Two kinds of radical capture reagents were employed in the WOR, and the results revealed that the main active species are sulfate radicals. Based on the results, the mechanism of CuO-OH as a catalyst in WOR was correspondingly proposed: the CuO-OH could activate persulfate to produce sulfate radicals which could oxidize water into oxygen by a deprotonation process.

ACKNOWLEDGEMENTS

We gratefully acknowledge the financial support from the National Natural Science Foundation of China (No. 21861035), The Regional Collaborative Innovation Project of Xinjiang Uyghur Autonomous Region (No. 2017E01005), The University Scientific Research Project of Xinjiang Uyghur Autonomous Region (No. XJEDU2017I001) and the National Natural Science Foundation of China (No. 21162027).

CONFLICT OF INTEREST

The authors declare that there are no financial and non-financial conflicts.

SUPPORTING INFORMATION

Additional information as noted in the text. This information is available via the Internet at http://www.springer.com/chemistry/journal/11814.

REFERENCES

1. T. Fang, L.-Z. Fu, L.-L. Zhou and S.-Z. Zhan, *Electrochim. Acta*, **161**, 388 (2015).
2. X. Liu, H. Zheng, Z. Sun, A. Han and P. Du, *ACS Catal.*, **5**, 1530 (2015).
3. A. Singh and L. Spiccia, *Coord. Chem. Rev.*, **257**, 2607 (2013).
4. M. Tabata, K. Maeda, T. Ishihara, T. Minegishi, T. Takata and K. Domen, *J. Phys. Chem. C*, **114**, 11215 (2010).
5. S. J. A. Moniz, S. A. Shevlin, D. J. Martin, Z.-X. Guo and J. Tang, *Energy Environ. Sci.*, **8**, 731 (2015).
6. I. Papadas, J. A. Christodoulides, G. Kioseoglou and G. S. Armatas, *J. Mater. Chem. A*, **3**, 1587 (2015).
7. Y. Y. Lu, Y. Y. Zhang, J. Zhang, Y. Shi, Z. Li, Z. C. Feng and C. Li, *Appl. Surf. Sci.*, **370**, 312 (2016).
8. J. Huang, X. Du, Y. Feng, Y. Zhao and Y. Ding, *Phys. Chem. Chem. Phys.: PCCP*, **18**, 9918 (2016).
9. P. A. Michaud, M. Panizza, L. Ouattara, T. Diaco, G. Foti and C. Comninellis, *J. Appl. Electrochem.*, **33**, 151 (2003).
10. R. Zong and R. P. Thummel, *J. Am. Chem. Soc.*, **127**, 12802 (2005).
11. W. C. Ellis, N. D. McDaniel, S. Bernhard and T. J. Collins, *J. Am. Chem. Soc.*, **132**, 10990 (2010).
12. T. S. Glikman and I. S. Shcheglova, *Kinet. Katal.*, **9**, 461 (1968).
13. N. D. McDaniel, F. J. Coughlin, L. L. Tinker and S. Bernhard, *J. Am. Chem. Soc.*, **130**, 210 (2008).
14. M. Z. Ertem and C. J. Cramer, *Dalton Trans.*, **41**, 12213 (2012).
15. T. An, H. Yang, G. Li, W. Song, W. J. Cooper and X. Nie, *Appl. Catal. B: Environ.*, **94**, 288 (2010).
16. A. Primo, T. Marino, A. Corma, R. Molinari and H. García, *J. Am. Chem. Soc.*, **133**, 6930 (2011).
17. H.-y. Liang, Y.-q. Zhang, S.-b. Huang and I. Hussain, *Chem. Eng. J.*, **218**, 384 (2013).
18. Y. Zhang, H. P. Tran, I. Hussain, Y. Zhong and S. Huang, *Chem. Eng. J.*, **279**, 396 (2015).
19. Y. Zhang, H. P. Tran, X. Du, I. Hussain, S. Huang, S. Zhou and W. Wen, *Chem. Eng. J.*, **308**, 1112 (2017).
20. I. Hussain, M. Li, Y. Zhang, S. Huang, W. Hayat, Y. Li, X. Du and G. Liu, *J. Environ. Chem. Eng.*, **5**, 3983 (2017).
21. I. Hussain, Y. Zhang and S. Huang, *RSC Adv.*, **4**, 3502 (2014).
22. X. Du, Y. Zhang, I. Hussain, S. Huang and W. Huang, *Chem. Eng. J.*, **313**, 1023 (2017).
23. J. Yang, H. Liu, W. N. Martens and R. L. Frost, *J. Phys. Chem. C*, **114**, 111 (2010).
24. L. Trotochaud, S. L. Young, J. K. Ranney and S. W. Boettcher, *J. Am. Chem. Soc.*, **136**, 6744 (2014).
25. O. Diaz-Morales, D. Ferrus-Suspedra and M. T. M. Koper, *Chem. Sci.*, **7**, 2639 (2016).
26. S. R. Alvarado, Y. Guo, T. P. A. Ruberu, A. Bakac and J. Vela, *J. Phys. Chem. C*, **116**, 10382 (2012).
27. J. Zhu, D. Li, H. Chen, X. Yang, L. Lu and X. Wang, *Mater. Lett.*, **58**, 3324 (2004).
28. C. Yang, X. Su, J. Wang, X. Cao, S. Wang and L. Zhang, *Sens. Actuators B: Chem.*, **185**, 159 (2013).
29. H. R. Naika, K. Lingaraju, K. Manjunath, D. Kumar, G. Nagaraju, D. Suresh and H. Nagabhushana, *J. Taibah Univ. Sci.*, **9**, 7 (2015).
30. A. Chauhan, R. Verma, K. M. Batoo, S. Kumari, R. Kalia, R. Kumar, M. Hadi, E. H. Raslan and A. Imran, *J. Mater. Res.*, **36**, 1496 (2021).
31. M. I. T.-T. a. M. A. Anderson, *Langmuir*, **2**, 203 (1986).
32. K.-C. Huang, R. A. Couttenye and G. E. Hoag, *Chemosphere*, **49**, 413 (2002).
33. K.-Y. A. Lin, B.-J. Chen and C.-K. Chen, *RSC Adv.*, **6**, 92923 (2016).